SCIENTIFIC REPORTS

OPEN

SUBJECT AREAS:
OPTICAL MANIPULATION AND TWEEZERS
BIOPHOTONICS
APPLIED OPTICS
FIBRE OPTICS AND OPTICAL COMMUNICATIONS

Received
28 August 2012

Accepted
18 October 2012

Published
12 November 2012

Correspondence and requests for materials should be addressed to B.L. (stslbj@mail.sysu.edu.cn)

Optical trapping, driving, and arrangement of particles using a tapered fibre probe

Hongbao Xin, Rui Xu & Baojun Li

State Key Laboratory of Optoelectronic Materials and Technologies, School of Physics and Engineering, Sun Yat-Sen University, Guangzhou 510275, China.

The ability of manipulating mesoscopic objects with high precision and flexibility is extremely important for a wide variety of fields from physics, biochemistry, to biomedicine. Particularly, the ability of arranging particles/cells into desired patterns precisely is a challenge for numerous physical and biological applications. Here, we report a strategy of realizing highly flexible trapping, driving, and precise arrangement of particles using a tapered fibre probe. Using randomly distributed 3-μm-diameter silica particles as an example, we demonstrate that the strategy is able to stably trap the particles and drive them to targeted regions, subsequently arrange the particles into desired patterns. To further demonstrate the ability of this strategy, experiments were done using sub-micron sized particles and biological samples (bacteria and cells). This strategy provides a new approach to manipulate mesoscopic objects precisely and flexibly, and hopefully can be used in future fundamental and applied researches of interdiscipline.

Since its first introduction[1], optical manipulation has boosted a rapid progress in science and engineering[2–7]. For example, the continued development of optical trapping has seen its unsubstitutive crucial role for research in the fields of soft condensed matter physics, biochemistry, clinical medicine, and is delivering new insights and discoveries[8–14]. Most of the intriguing results are achieved with conventional optical tweezers (COTs) based on standard microscopes by focusing free space light beams using high-numerical-aperture (high-NA) objective. Objects ranging in size from tens of nanometers such as proteins[15] and DNA molecules[16], to tens of micrometers such as colloidal particles[4], can be trapped and moved by a strongly focused light beam. Because of the targeted and noninvasive nature, COTs are extensively used in biochemical and biophysical researches. Although innovation in COTs is increasingly being made along with other micro/nanotechnology, the relatively bulky structure of the focusing objective and optical system make it lacking of flexibility in moving and focusing. In addition, it also has limitations in the application of thick samples because of the difficulty in penetrating thick samples by focus generated by the objective.

With the advantages of easy fabrication and high flexibility, fibre optical tweezers (FOTs)[17–19] are attracting increasing attention as a new powerful tool for mesoscopic object trapping and manipulation. Because of avoiding the use of high-NA objective, FOTs are becoming miniaturized, versatile, and handy tools for particle trapping and manipulation[20]. Moreover, single optical fibre can also be used to trap particles by photothermal effect[21] or to drive objects by scattering force[22,23]. However, above mentioned single fibre is used with only a single function, either trapping or driving of particles. Nevertheless, combining both function of trapping and driving in a single fibre is of great importance because it can trap biological samples and drive them to a designated position in a microfluidic system or a vessel. In addition, particle arrangement with high precision is also important for biological applications and biophotonic integration[24,25]. Using a single optical fibre, patterns of microparticles and cells can be realized[17]. However, FOTs are typically used to trap and manipulate particles with several microns in size. They are difficult to trap and manipulate sub-micron sized particles because of obvious Brownian motion of particles. COTs assisted methods, such as holographic optical tweezers (HOTs)[26–30] and surface plasmon-based optical tweezers (SPOTs)[13,14,31,32], have also been used in particle arrangement. Unfortunately, for HOTs, bulky optical system and appropriate algorithms for phase hologram calculation on a desired pattern are needed, while a carefully designed lithographic substrate is also needed for SPOTs, making it difficult for arranging particles with any desired configuration.

To realize the combination of trapping, driving, and arrangement ability, in this work, we report a tapered fibre probe (TFP)-based strategy for highly precise and flexible manipulation of mesoscopic objects, which successfully

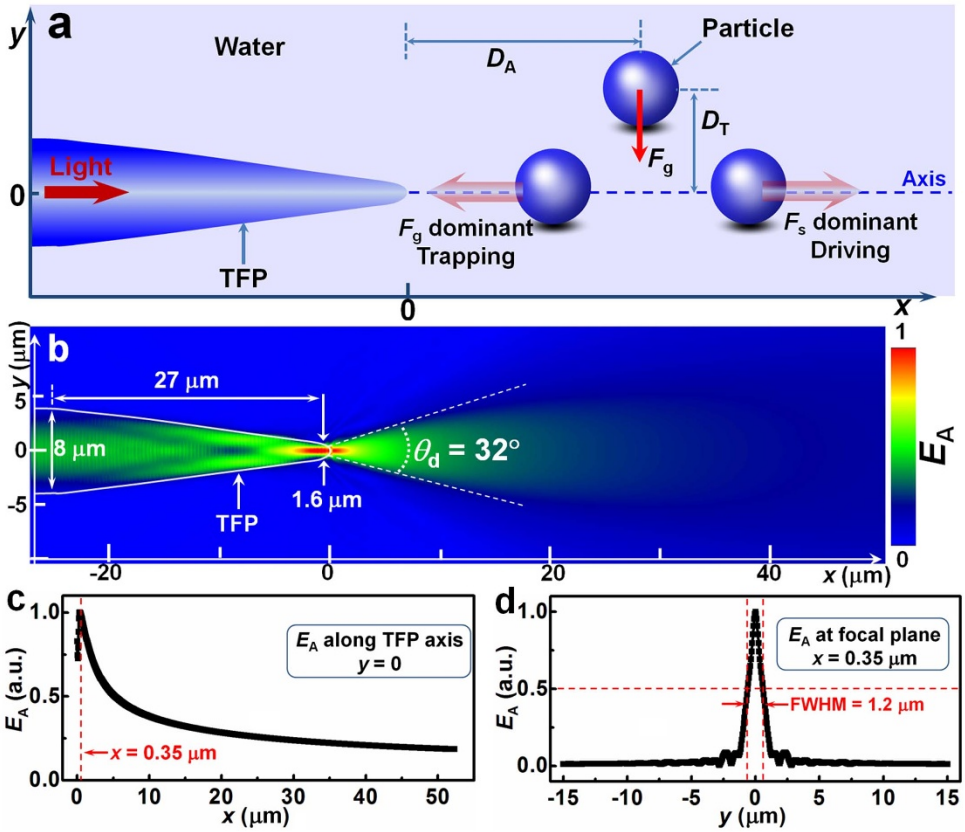

Figure 1 | Model and simulated electric field amplitude (E_A) distribution. (a) Schematic of particle manipulation by a TFP with light launched. (b) FDTD simulated E_A. (c) Normalized E_A along the TFP axis ($x \geq 0$, $y = 0$). (d) Normalized E_A at the focal plane ($x = 0.35$ μm).

combines the ability of trapping, driving, and arrangement of particles. The trapped particles can be flexibly moved to any desired position with high precision and arranged into desired patterns. Using randomly distributed 3-μm-diameter silica particles as an example, the particles have been trapped and positioned in specific positions, driven to targeted regions, and arranged into desired patterns. The manipulation ability has also been extended to sub-micron particles and biological samples (bacteria and cells).

Results

Theoretical simulations and calculations. Figure 1a schematically shows a TFP immersed in water. D_A and D_T indicate the axial distance (in x direction) and transverse distance (in y direction) of a dispersed particle to the TFP tip and the axis, respectively. Once a light beam is launched into the TFP, particles irradiated by the light outputted from the TFP will be manipulated by the optical force exerted on them. The optical force consists of a gradient force (F_g: directing to stronger light intensity region to trap particles) and a scattering force (F_s: in the direction of light propagation to drive particles away from the stronger light intensity region). Resultant force of F_g and F_s dominates trapping or driving of the particles. For the particle beside the axis, it will be trapped to the axis by F_g. For the particle along the axis and near the tip, F_g is much stronger than F_s, therefore, it will be trapped to the TFP tip by F_g. As the distance to the tip increases, F_g gradually becomes smaller than F_s, as a result, particle will be driven away by F_s. By using finite-difference time-domain (FDTD) simulations, the electric field amplitude (E_A) distribution around the TFP was obtained and shown in Fig. 1b. To get an obvious trapping and driving performance, and meanwhile, induce little harm on the particles or biological samples, the wavelength of launched light is set to be 980 nm (with an excitation power of 1 W/m). Silica particles with 3-μm diameter are used as an example in the simulation. The diameter of the TFP (immersed in water) is set to be 8 μm at the input port, then linearly decreased to 1.6 μm within 27-μm-length, and ended with a parabolic end. The refractive indices of the TFP and water are set to be 1.45 and 1.33, respectively. It can be seen from Fig. 1b that the light outputted from the TFP is firstly focused at the tip and subsequently diverged out in water with a divergence angle of 32°. Figure 1c shows the E_A out of the TFP along the TFP axis in x direction ($y = 0$). It can be seen that the focal plane (with the strongest light intensity) is away from the tip at $x = 0.35$ μm. Figure 1d shows the E_A at the focal plane in y direction ($x = 0.35$ μm). It can be seen that the light intensity at the focus is much stronger than that outside the focus. The full width at half maximum (FWHM) is 1.2 μm. Because the light is strongly focused at the TFP tip, thus particles near the tip will be exerted with a large F_g and be trapped by the TFP. As distance D_A to the TFP increases, the light intensity gradually decreases, and thus F_s gradually becomes larger than F_g, as a result, the particles will be driven away.

To numerically show trapping and driving performance, the optical force exerted on a particle was calculated by taking the integral of Maxwell stress tensor around the particle (see Supplementary Information for details)[18,33]. Figure 2a shows the calculated force F_x exerted on the particle located at different D_A along the TFP axis (i.e. $D_T = 0$). It can be seen that near the TFP tip ($D_A < 13$ μm), F_x is negative, indicating a trapping force directing to the TFP. In this region, the dominant force is gradient force F_g. All the particles in this region will be trapped. Therefore, the region is called trapping region (R_T). In R_T, F_x is decreased from −319.9 to −996.8 pN/W with an increase of D_A from 2 to 4.5 μm, and then increased from −996.8 to −9.8 pN/W with an increase of D_A from 4.5 to 13 μm. The largest trapping force is occurred at $D_A = 4.5$ μm. It should be pointed out that particle at around the position $D_A = 13$ μm cannot

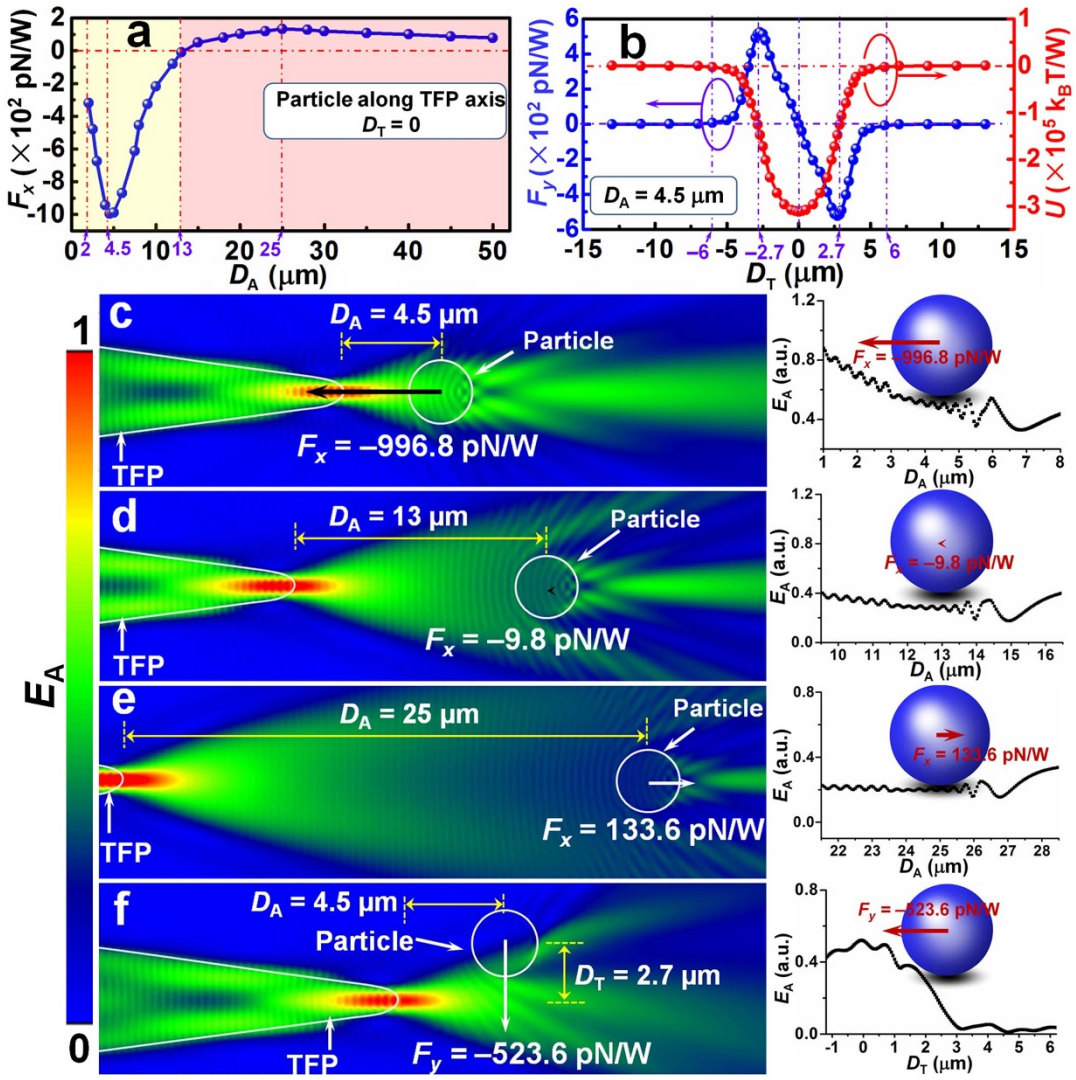

Figure 2 | Calculated optical force and simulated E_A distribution. (a) Axial force (F_x) exerted on particles along the TFP axis, yellow and red regions indicate the trapping and driving regions, respectively. (b) Transverse force (F_y) and trapping potential (U) for particles at $D_A = 4.5$ μm. (c) E_A for particle at $D_A = 4.5$ μm. (d) E_A for particle at $D_A = 13$ μm. (e) E_A for particle at $D_A = 25$ μm. (f) E_A for particle at $D_A = 4.5$ μm and $D_T = 2.7$ μm. Right panels show corresponding E_A distributions through particle along the TFP axis (for (c), (d), and (e)) and $x = 4.5$ μm (for (f)).

be manipulated by the TFP. This is because F_x is about 0 (F_g is balanced with F_s in this location). For particles located at $D_A > 13$ μm, F_x is positive, indicating a driving force directing to the light propagation direction. In this region, since the dominant force is scattering force F_s, particles will be driven away. Therefore, the region is called driving region (R_D). In R_D, F_x is firstly increased because of the increasing difference between F_s and F_g. At $D_A = 25$ μm, F_x reaches the maximum (133.6 pN/W). At $D_A > 25$ μm, F_x is gradually decreased with increasing D_A, ascribing to the decrease of light intensity. Thus, particles far away from the tip also cannot be manipulated. The transverse force (F_y) was also calculated. Figure 2b, as an example, shows the calculated F_y (blue-dotted curve) as a function of transverse distance (D_T) for particles located at $D_A = 4.5$ μm. It can be seen that, F_y exhibits a symmetrical distribution. This is because light distribution is symmetrical relative to the TFP axis. It can also be seen that, far away from the axis ($|D_T| > 6$ μm), F_y is very small because of the weak light intensity and thus particles cannot be manipulated. Once particles gradually get close to the axis, $|F_y|$ is gradually increased until reaches the maximum of 523.6 pN/W at $|D_T| = 2.7$ μm, then gradually decreased from 523.6 to 0 pN/W as $|D_T|$ is decreased from 2.7 to 0 μm. By integrating F_y over distance, the trapping potential (U) was obtained as shown by red-dotted curve in Fig. 2b. It can be seen that the calculated U reaches the minimum at $D_T = 0$ μm. This means that the particles near the TFP axis can be trapped to the axis. Figures 2c-e show the simulated E_A distribution for particles along the TFP axis at $D_A = 4.5$, 13, and 25 μm, respectively. It can be seen that, for $D_A = 4.5$ μm, light intensity is stronger on the left side (illuminated side) than that on the right side (shaded side). This is because the particle is near the focus. Thus F_x directs to the TFP (Fig. 2c). For $D_A = 13$ μm, light intensities on both the left and right sides of the particle are almost equal and F_x is only −9.8 pN/W (Fig. 2d). For $D_A = 25$ μm, light intensity on the right side is larger than that on the left side because of the refocusing of light by the particle, thus F_x directs to the direction of the light propagation. E_A distribution for the particle at $D_A = 4.5$ μm and $D_T = 2.7$ μm is shown in Fig. 2f. It can be seen that light intensity is much stronger on the side near the TFP axis. Thus F_y directs to the axis and the particle will be trapped to the axis. Since particles suspended in water can be efficiently trapped and/or driven away by a TFP, therefore, once the TFP is moved, the particles can be trapped, driven, and arranged with high precision and flexibility.

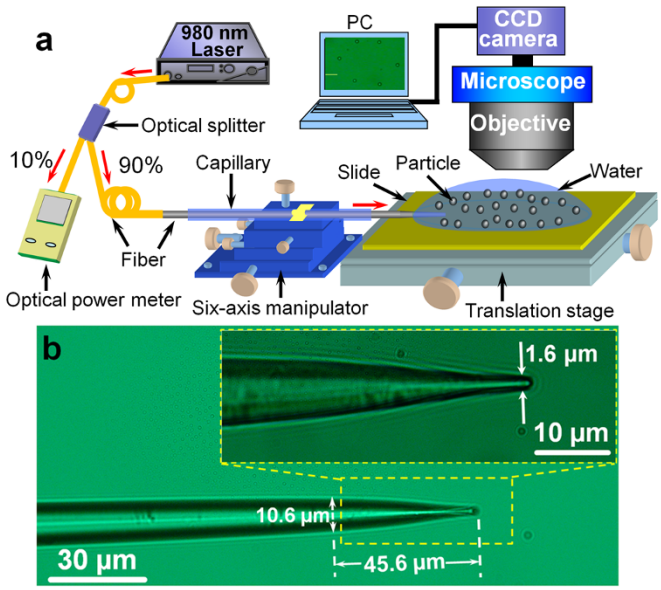

Figure 3 | Experimental setup. (a) Schematic of experimental setup, a 980-nm laser is split into two parts with 10% connected to an optical power meter and 90% injected into the TFP which is immersed in a silica particle suspension. The fibre is sheathed by a glass capillary and manipulated by a six-axis manipulator. All the experimental data can be obtained by a personal computer (PC) interfaced microscope with a CCD camera. (b) Optical microscope image of the TFP. Diameter of the TFP is decreased from 10.6 to 1.6 μm within 45.6-μm axial distance.

Trapping and driving of particles. Based on the above analysis, an experimental setup was designed and built as shown in Fig. 3a. To trap and drive particles, a laser of 980-nm wavelength was launched into the TFP (Fig. 3b, see Methods for fabrication), which was fixed by a 3-demensional (3D) six-axis manipulator (see Methods for description). The tip of the TFP was immersed in the particle suspension (3-μm-diameter silica particle, see Methods for preparation). Figure 4 shows a sequence of optical microscope images for trapping and driving of particles by the TFP. Figure 4a shows that without light launched into the TFP, particles were randomly suspended in water. Among them, particles A, B, and C were near the TFP tip. Inset of Fig. 4a schematically shows D_A and D_T which indicate the location of the particle. With an optical power of 18 mW launched into the TFP, particle A (D_A = 5.7 μm, D_T = 0 μm) was kept static, while particle B (D_A = 13.8 μm, D_T = 4.2 μm) was firstly trapped to the TFP axis with a moving distance of 4.2 μm in y direction within 0.55 s by the gradient force F_g (Fig. 4b), consistent with the simulations and calculations for transverse gradient force shown in Fig. 2b. An average of F_g = 0.19 pN was calculated according to the Stokes' drag formula: $F = 6\pi r\eta v$, where r = 1.5 μm is the particle radius, $\eta = 8.9\times10^{-4}$ Pa·s is the dynamic viscosity of water at room temperature, and v is the particle velocity (here 7.6 μm/s)[34]. Particle C was kept static in the whole process, it was likely the result of particle sticking to the glass slide. After particle B was trapped to the axis, the TFP was then gradually moved in $-y$ direction. In this process, particle A and particle B (here D_A = 13.8 μm, D_T = 0 μm) were also moved by the transverse gradient force along with the move of the TFP in $-y$ direction. At t = 1.31 s, both particles A and B were moved with a distance of 5.8 μm (Fig. 4c). By further increasing the optical power from 18 to 40 mW, particle A was trapped to the tip by the dominant F_g (0.26 pN from calculation) at an average velocity of 10.2 μm/s, while particle B was driven 5.2 μm away within 0.41 s in x direction by the dominant F_s (0.32 pN from calculation) with an average velocity of 12.7 μm/s (Fig. 4d). This is consistent with the simulations and calculations for particles in the trapping and driving regions shown in Fig. 2a. Note that, because there was a little difference of TFP profile between the model in simulation and that in experiments. In simulation, the model of TFP is assumed with an axisymmetric profile and a parabolic end, but in experiment, it is hardly to fabricate a TFP with an ideal profile as that assumed in the simulation because of ambient interference during the fabrication process. Since optical field (and thus optical force) distribution strictly depends on the TFP profile, thus the actual optical force exerted on the particles and the range of trapping and driving regions differ a little from that obtained from

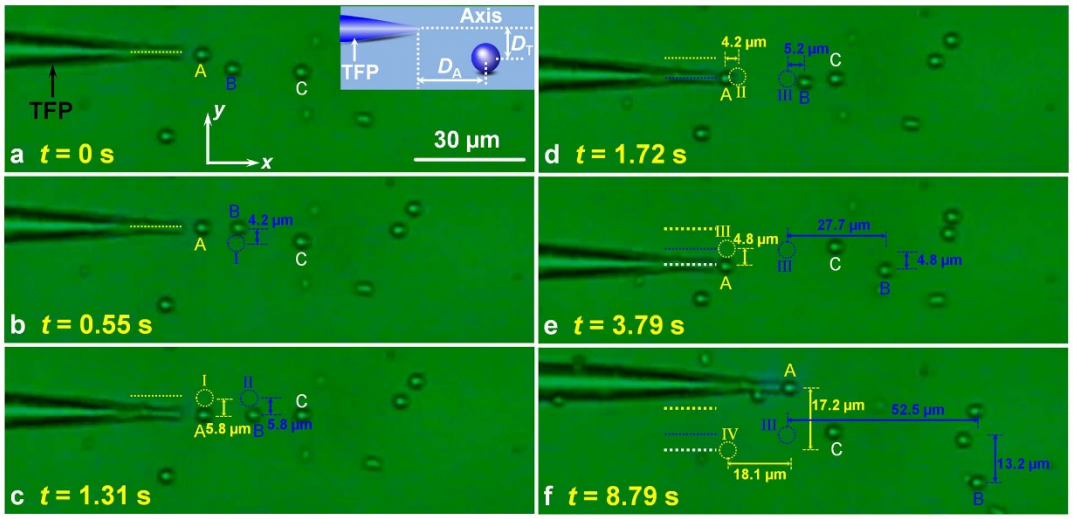

Figure 4 | A sequence of optical microscope images recorded for trapping and driving of particles by TFP. (a) t = 0 s, without light launched into the TFP, yellow dashed line indicates the original location of the TFP. Particles A, B, and C were randomly suspended. Inset schematically shows the location of a particle. (b) TFP launched with an optical power of 18 mW (980-nm wavelength) for t = 0.55 s, Particle B was trapped to the axis in y direction, blue circle I indicates the location of particle B in panel (a). (c) t = 1.31 s, particles A and B were moved in $-y$ direction, yellow circle I and blue circle II indicate the respective locations of particles A and B in panel (b). (d) t = 1.72 s, power increased to 40 mW, particle A was trapped and particle B was driven away, yellow circle II and blue circle III indicate the locations of particles A and B in panel (c). (e) For t = 3.79 s, yellow circle III, blue dashed line, and white dashed line indicate the locations of particle A in panel (d), TFP in panel (d), and TFP in panel (e), respectively. (f) For t = 8.79 s, yellow circle IV indicates the location of particle A in panel (e). Particle C kept static in the whole process.

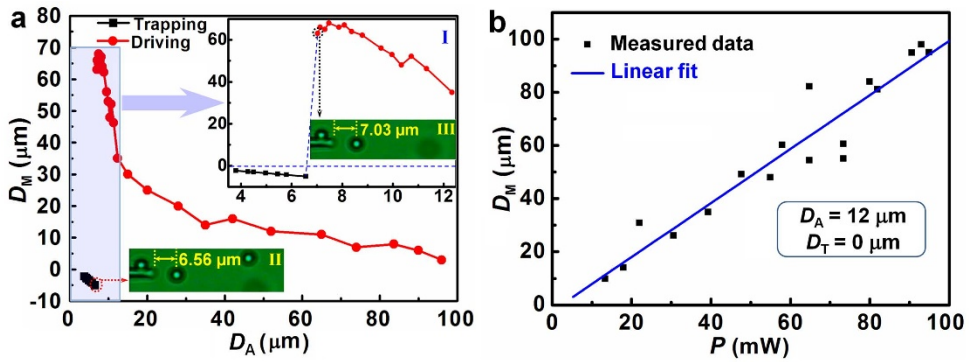

Figure 5 | Trapping and driving ability. (a) Manipulation distance (D_M) for particles as a function of D_A ($D_T = 0$ μm). Negative values indicate particles being trapped, while positive values for driven. Inset I is a detailed description of the light blue region. Insets II and III show the images for the trapping and driving performance with $D_A = 6.56$ and 7.03 μm, respectively. (b) D_M as a function of input optical power (P) for particles at $D_A = 12$ μm and $D_T = 0$ μm. Linear fit shows D_M increases with increasing P.

simulation shown in Fig. 2. As the TFP was continuously moved in $-y$ direction, the trapped particle A was also moved along with the TFP. Interestingly, particle B was also moved in $-y$ direction with the move of the TFP by the transverse gradient force, and at the same time, was driven away in $+x$ direction by the axial scattering force. Figure 4e shows that, at $t = 3.79$ s, particle A was moved 4.8 μm in $-y$ direction, while particle B was moved 27.7 and 4.8 μm in x and $-y$ directions, respectively. As shown in Fig. 4f, with the move of the TFP, particle A was moved 18.1 and 17.2 μm in x and y directions, respectively. However, as the TFP was moved far away, light intensity (and thus optical force) irradiated on particle B was quickly decreased to zero as shown in Figs. 1d and 2b, thus particle B was not trapped to the axis of the TFP. As a result, particle B was moving away in the original direction. At $t = 8.79$ s, particle B was driven away with distances of 52.5 and 13.2 μm in x and $-y$ directions, respectively. Detailed trapping and driving process is shown in Supplementary Video S1. Further experiments show that, multiple particles can also be manipulated (see Supplementary Fig. S1 and Supplementary Video S2).

To show the trapping and driving ability of the TFP, experiments on manipulation distance (D_M) for particles at different D_A were performed (keeping the particles along the axis of the TFP, i.e. $D_T = 0$ μm). When keeping the input power at 40 mW, experimental results show that, at $D_A \leq 6.56$ μm (F_g dominant), particles were trapped by the TFP, while at $D_A \geq 7.03$ μm (F_s dominant), particles were driven away (Fig. 5a). At $D_A = 6.56$ μm (the largest D_A for particle trapping observed in the experiments, inset II), the particle can be trapped to the tip in 0.27 s with an average velocity of 18.7 μm/s (see Supplementary Video S3). At $D_A = 7.03$ μm (the smallest D_A for driving observed in the experiments, inset III), the particle was firstly driven away with an average velocity of 9.1 μm/s in the first 2 seconds, and then gradually decrease to 0 by the decreasing F_s generated by the decreasing light intensity (see Figs. 1c and 2a), and finally stopped after 24.5 s with a manipulation distance (D_M) of 63 μm (see Supplementary Video S4). The difference between the observed largest trapping D_A and the smallest driving D_A was only 470 nm. D_M quickly decreases when $D_A > 7.03$ μm, far away from the TFP, D_M gradually tends to 0. The reason is that F_s decreases quickly in the weak light region, and finally tends to 0 (see Fig. 2a). To show the dependence between the driving ability and input optical power (P), a series of experiments were performed for particles at $D_A = 12$ μm and $D_T = 0$ μm. Results show that D_M is almost linearly increased with P (Fig. 5b) because of the increasing optical force induced by the increasing optical intensity.

Arrangement of particles. By combining the trapping and driving performance, the TFP can be easily used for particle positioning and arrangement with high precision and flexibility with a launched light at 980-nm wavelength. Images from left to right (Fig. 6a) show a process of arranging six particles to form a hexagon. Each particle was picked up and trapped by the TFP with a launched optical power of 25 mW and subsequently positioned at a desired position to form a vertex of the hexagon. Supplementary Fig. S2 and Supplementary Video S5 show the detailed process of pick-and-position of the sixth particle to form the sixth vertex of the hexagon. Images from left to right (Fig. 6b) show the process of arranging six randomly suspended particles to form a triangle. Particles were sequentially driven by the TFP at an optical power of 35 mW to a desired position to form the sides of the triangle (see Supplementary Video S6 for details). By combining the trapping and driving ability, desired patterns can be arranged. Images from left to right (Fig. 6c) show a line, a parallelogram, a pentagon (the upper two particles sticking together), a jointed threefold pattern, and a disjointed threefold pattern formed by four, four, six, four, and six particles, respectively. Images from left to right (Fig. 6d) show the arranged letters "T", "D", and "A" for "Trapping", "Driving", and "Arrangement", respectively, and "S", "Y", and "U" for "Sun Yet-Sen University".

Besides the positioning and arrangement of particles, the versatile nature of the TFP can also be used for other applications. For example, randomly suspended particles can be delivered to a targeted region using the trapping and driving ability of the TFP (see Supplementary Fig. S3).

Discussion

The above experimental results show that the TFP can be flexibly used for trapping and driving of particles with different working distance. These results corroborate our theoretical analysis and numerical calculation. To investigate the effect of particle size on this method, calculations of optical force (F_x) exerted on particles with different sizes (0.7/3/5-μm-diameter SiO_2 and 10-μm-diameter polystyrene (PS) particles) along the TFP axis were carried out as shown in Fig. 7a. It can be seen that, the trapping (negative F_x values indicated) and driving (positive F_x values indicated) ability are applicable to particles with different diameters, from sub-micron to ~10 microns. It can also be seen that, for a larger particle, the trapping region is larger than that for a smaller one. Although it is difficult to extract quantitative values for trapping stability experimentally, from the numerical calculations, one can estimate the trapping efficiency (Q) which is defined by $Q = cF/n_M P$, where c is the velocity of light in vacuum, F is the optical force (i.e. the calculated F_x), n_M is the refractive index of surrounding medium (water), and P is the input optical power[20]. The calculated maximum trapping efficiencies are 0.181, 0.224, and 0.231 for the 0.7-, 3-, and 5-μm-diamter SiO_2 particles, respectively, and 0.227 for the 10-μm-diameter PS

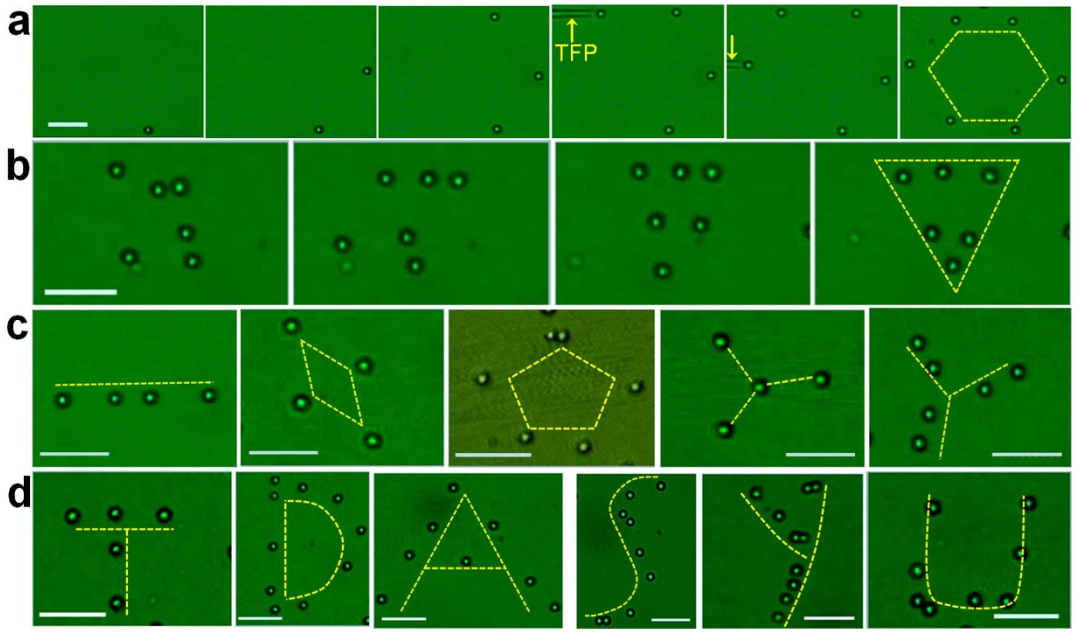

Figure 6 | Images of particle positioning and arrangement. (a) From left to right is sequential arrangement of a hexagon with 6 particles. The yellow arrows indicate the TFP. (b) Sequential arrangement of a triangle with 6 particles. (c) Arrangement of a line, a parallelogram, a pentagon, a jointed threefold pattern, and a disjointed threefold pattern, respectively. (d) Arrangement of letters "T" for Trapping, "D" for Driving, "A" for Arrangement, and "S", "Y", and "U" for "Sun Yat-Sen University". Scale bars are 20 μm.

particles. As an example of comparison, for the 10-μm-diameter PS particles, calculated $Q = 0.227$ for this method is higher than the $Q = 0.12 \pm 0.014$ for COTs method reported by Wright *et al.*[35] and $Q = 0.195$ for FOTs method reported by Liberale *et al*[20].

To test the trapping and driving ability of the TFP for particles with different sizes and materials, experiments were further performed using 0.7-μm-diameter SiO_2 particles, yeast cells (average diameter: 4 μm), and *Escherichia coli* (*E. coli*) bacteria (rod-shaped, about 0.7 × 2 μm) as shown in Fig. 7b–d. These three kinds of particles can be trapped by the TFP when they were near the TFP (see Fig. 7bI–dI for trapping), and be driven away when they were with a larger distance away from the TFP (see Fig. 7bII–dII for driving). Experimental results show that the trapping and driving ability of the TFP is not only applicable for microparticles but also applicable for sub-micron sized particles and biological samples. Note that, Brownian motion is much more obvious for sub-micron sized particles than that for micron sized particles, therefore, a higher optical power is needed to exert a large optical force to suppress the Brownian motion. Compared to the reported results with FOTs (for trapping of particles with several microns in size)[17–20], the TFP has advantages in manipulating objects in size from sub-micron to several microns and even particle clusters, and with materials from dielectric particles to bacteria and cells. Moreover, multi-purpose of stable trapping, targeted driving, and precise arrangement of particles can also be achieved using the TFP. Detailed comparison between the TFP and FOTs methods is listed in Supplementary Table S1.

Compared to the COTs methods, the presented TFP trapping is advantaged in multiple functions, suspension applicability, manipulation flexibility, precision, and trapping stability. (1) The TFP can be used for stable trapping, flexible moving, targeted driving, and precise arrangement of particles. COTs are generally used for stable trapping and moving of particles. To realize precise arrangement, additional holographic optical tweezers or surface plasmon-based optical tweezers are needed in COTs. (2) The TFP can be inserted into particle suspensions with different directions and depths. For COTs method, it is difficult to generate a focus with different directions and depths in thick suspensions[20]. (3) Trapped particles can be delivered to any designated positions using the TFP by manipulating the six-axis manipulator (see Fig. 4 and Fig. S2). To manipulate trapped particles using the COTs, one should control the focus through beam steering and amplitude modulation elements incorporated in the optical path before the laser beam enters the high-NA objective[36]. Therefore, TFP is more flexible. (4) The resolution of the six-axis manipulator which used for fixing the TFP is 50 nm, thus the manipulation precision of the TFP method can be reached to 50 nm. While for the COTs, to move the trapped particles, one should control the focus through a bulky optical system with a series of lens for beam steering and amplitude modulation[36]. Therefore, COTs method is less precise for moving. (5) By comparing the calculated trapping efficiency (Q) which determines the trapping stability, the TFP trapping is more stable than that of the COTs trapping. Using 10-μm-diameter PS particles as an example, the calculated Q are 0.227 and 0.12 for the TFP and COTs trapping, respectively. It should be emphasized that the COTs trapping is a noncontact method with large particle universality and capable of trapping particles in size ranging from tens of nanometers to tens of micrometers with materials from dielectric to biological particles[4]. The TFP method is a contact trapping with particle sizes from sub-micron to several microns (even particle clusters) and materials from dielectric particles to biological samples (bacteria and cells), we have not performed stable trapping of particles with size less than 500 nm. Detailed comparison is also listed in Supplementary Table S1.

Compared to the HOTs methods which are normally used for particle arrangement, the TFP based arrangement is advantaged in system simplicity, flexibility, and trapping stability in each trap. (1) To arrange particles, the key part is a fibre for the TFP method while for the HOTs method, a high-NA objective, relay lens, and a diffractive optical element (DOE, used to imprint a computer-generated hologram) are essential[26,28]. Therefore, the TFP system is much simpler. (2) By using TFP, particles can be trapped and delivered to designated positions (see Supplementary Fig. S2), or directly driven to designated positions (Fig. 6b). Therefore, any desired patterns can be arranged. While for HOTs arrangement,

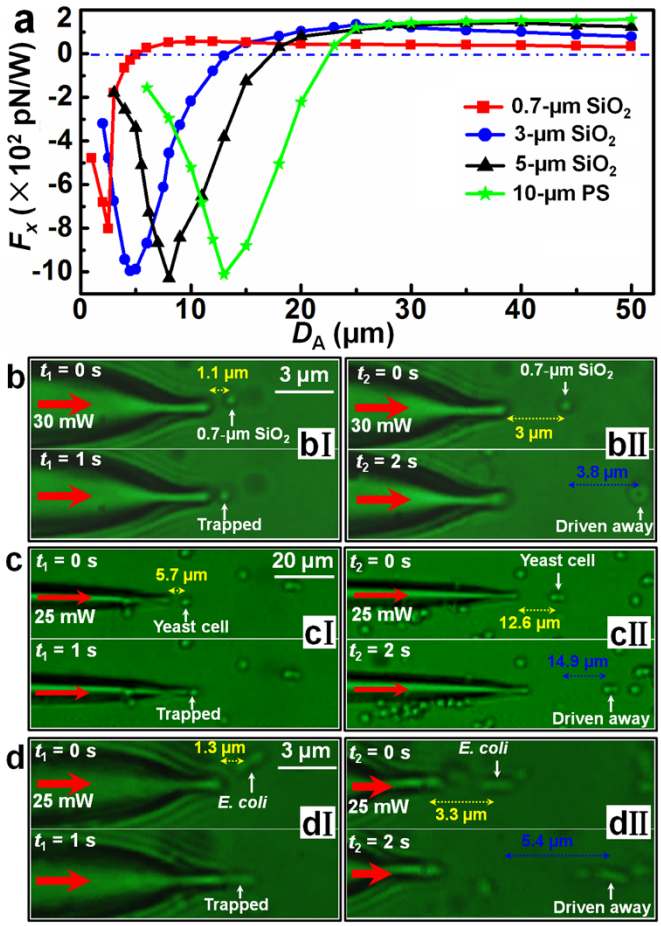

Figure 7 | Trapping and driving ability for different particles. (a) Calculated optical force (F_x) for 0.7/3/5-μm-diamter SiO_2 and 10-μm-diameter polystyrene (PS) particles as a function of axial distance (D_A) to the TFP. (b)–(d) Optical microscope images for trapping and driving of particles with different sizes and materials. (b) Trapping and driving of 0.7-μm-diameter SiO_2 particles with an optical power of 30 mW. (bI) For trapping, at trapping time $t_1 = 0$ s, the particle was 1.1 μm away from the TFP. At $t_1 = 1$ s, the particle was trapped; (bII) For driving, at driving time $t_2 = 0$ s, the particle was 3 μm away from the TFP. At $t_2 = 2$ s, the particles was driven away with 3.8 μm. (c) Trapping and driving of yeast cells with an optical power of 25 mW. (cI) For trapping, at $t_1 = 0$ s, the cell is 5.7 μm away from the TFP. At $t_1 = 1$ s, the cell was trapped; (cII) For driving, at $t_2 = 0$ s, the cell was 12.6 μm away from the TFP. At $t_2 = 2$ s, the cell was driven away with 14.9 μm. (d) Trapping and driving of *E. coli* with an optical power of 25 mW. (dI) For trapping, at $t_1 = 0$ s, the *E. coli* was 1.3 μm away from the TFP. At $t_1 = 1$ s, the *E. coli* was trapped; (dII) For driving, at $t_2 = 0$ s, the *E. coli* was 3.3 μm away from the TFP. At $t_2 = 2$ s, the *E. coli* was driven away with 5.4 μm.

to form a specific pattern, a specific algorithm for phase hologram should be designed and prepared in advance. To achieve other patterns, corresponding algorithms should also be redesigned. Therefore, the TFP is more flexible in arranging different patterns. (3) In HOTs arrangement, a laser beam will be divided into multiple optical traps by the DOE, therefore, Q is about 0.05 for microparticles in each trap[28]. By using the TFP method, Q can be reached to 0.1~0.3. Therefore, trapping stability of the TFP method is higher. It should also be emphasized that in the HOTs arrangement, all particles are patterned at the same time[26], thus retaining ability of the patterned particles is higher than that in the TFP arrangement in which patterns are completed by positioning particles one by one and the patterned particles might be influenced by the particle Brownian motion and environment fluctuation. Detailed comparison is listed in Supplementary Table S2.

Compared to the SPOTs methods, the TFP arrangement is also advantaged in system simplicity and flexibility. (1) For the SPOTs arrangement, a carefully designed lithographic structured substrate and a high-NA objective are essential[14,15], thus the system is more complex than that in the TFP arrangement with a single fibre. (2) Since the patterns are decided by the carefully designed lithographic substrate in SPOTs arrangement, thus to arrange particles with different patterns, different substrate should be designed, while these patterns can be realized with a single fibre in TFP arrangement. Therefore, the TFP is more flexible to arrange different patterns. However, the SPOTs method is advantaged in both trapping stability and retaining ability. Benefiting from the localized Plasmon resonances of the nanostructured substrates, the peak Q are 14.0, 1.6, and 0.1 for 6 μm, 1 μm, and 200 nm particles, respectively in each trap[14]. This is much higher than the Q for HOTs method (~0.05 for microparticles[28]) and TFP method (0.1~0.3 for microparticles). Moreover, particles can be patterned at the same time using the SPOTs and the retaining ability is higher than that in the TFP arrangement. Detailed comparison is also listed in Supplementary Table S2.

In conclusion, a strategy of realizing highly flexible trapping, driving, and precise arrangement of particles with a tapered fibre probe has been demonstrated and analyzed with numerical calculation. Using randomly distributed 3-μm-diameter silica particles as an example, we demonstrate that the strategy is able to stably trap the particles and/or drive them to targeted regions, subsequently position the particles to certain specific positions, and arrange into desired patterns. Using 0.7-μm-diameter silica particles, yeast cells and *E. coli* as examples, we further demonstrate that the trapping and driving ability using the TFP is also applicable for sub-micron sized particles and biological samples (cells and bacteria), etc. The wide applicability of this strategy provides a new way to manipulate mesoscopic objects precisely and flexibly, and could be used in future interdisciplinary fundamental and applied researches.

Methods

Fabrication of TFP. The tapered fibre probe (TFP) was fabricated by drawing a commercial single-mode optical fibre (connector type: FC/PC, core diameter: 9 μm, cladding diameter: 125 μm, Corning Inc.) through a flame-heating technique. Before drawing, the polymer jacket of the fibre was stripped off with a fibre stripper to fabricate a bare fibre of 160-mm in length and 125-μm in diameter. The bare fibre was then sheathed by a glass capillary (inner diameter: ~0.9 mm, wall thickness: ~0.1 mm, length: ~120 mm). The bare fibre outside the capillary was used for drawing with a heating zone of about 2~3 mm. The drawing speed was firstly kept at about 0.3 mm/s, and the bare fibre diameter was decreased from 125 μm to 10 μm with a length of about 2 mm. Then a high speed of 2 mm/s was applied until the fibre broke with a highly tapered end. To make sure the TFP straight immersed into the particle suspension, the location of the capillary was adjusted until the TFP outside the capillary was 1.5 mm. Then the capillary with the bare fibre through it was fixed on a six-axis manipulator (Kohzu Precision Co., Ltd., 50 nm in resolution) and the TFP was straightly immersed into the suspension.

Description of experimental setup. The experimental setup is shown in Fig. 3a. A personal computer interfaced microscope with a charge-coupled device (CCD) is used for real-time monitoring and image capture. The microscope (Union, Hisomet II) consists of a series of objectives. The specifications of objective, including magnification, numerical aperture (NA) and working distance (WD), are ×5 (NA = 0.10, WD = 19.0 mm), ×10 (NA = 0.20, WD = 16.4 mm), ×20 (NA = 0.40, WD = 11.2 mm), ×40 (NA = 0.50, WD = 10.0 mm), ×50 (NA = 0.75, WD = 1.5 mm), and ×100 (NA = 0.73, WD = 1.0 mm). 980-nm wavelength laser from the laser source is coupled into an optical splitter, the optical power is measured by the 10% end which is connected to an optical power meter, and light from the 90% end is launched into the TFP, which was immersed in a water suspension of silica particles. The fibre sheathed by a glass capillary can be flexibly manipulated by the six-axis manipulator in 3D, thus the TFP including trapped and/or driven particles can be manipulated in 3D. To get a better manipulation result, the suspension above a glass slide can be further positioned by an *x-y* manual translation stage (resolution: 50 nm). Combining the manipulation of the six-axis manipulator and translation stage, the trapped and/or driven particles can be flexible and precisely manipulated in 3D, and thus can be used for particle arrangement.

Preparation of particle suspension. The suspension was prepared by diluting the particles with deionized water with additional ultrasonic treatment for 10 mins to get a monodisperse particle suspension. The concentration (weight ratio of particles to water) for the suspension is about 1 : 2,000. After preparation, the suspension was injected on a glass slide with a micro-syringe.

1. Ashkin, A. Acceleration and trapping of particles by radiation pressure. *Phys. Rev. Lett.* **24**, 156–159 (1970).
2. Grier, D. G. A revolution in optical manipulation. *Nature* **424**, 810–816 (2003).
3. Dholakia, K. & Reece, P. Optical micromanipulation takes hold. *Nano Today* **1**, 18–27 (2006).
4. Ashkin, A. Optical trapping and manipulation of neutral particles using lasers. *Proc. Natl. Acad. Sci. USA* **94**, 4853–4860 (1997).
5. Shvedov, V. G. *et al.* Giant optical manipulation. *Phys. Rev. Lett.* **105**, 118103 (2010).
6. Dholakia, K., Reece, P. & Gu, M. Optical micromanipulation. *Chem. Soc. Rev.* **37**, 42–55 (2008).
7. Moffitt, J. R., Chemla, Y. R., Smith, S. B. & Bustamante, C. Recent advances in optical tweezers. *Annu. Rev. Biochem.* **77**, 205–228 (2008).
8. Min, T. L. *et al.* High-resolution, long-term characterization of bacterial motility using optical tweezers. *Nat. methods* **6**, 831–835 (2009).
9. Ou-Yang, H. D. & Wei, M. T. Complex fluids: Probing mechanical properties of biological systems with optical tweezers. *Annu. Rev. Phys. Chem.* **61**, 421–440 (2010).
10. Liu, H., Newton, G. J., Nakamura, R., Hashimoto, K. & Nakanishi, S. Electrochemical characterization of a single electricity-producing bacterial cell of shewanella by using optical tweezers. *Angew. Chem.* **122**, 6746–6749 (2010).
11. Eriksson, E. *et al.* A microfluidic device for reversible environmental changes around single cells using optical tweezers for cell selection and positioning. *Lab Chip* **10**, 617–625 (2010).
12. Stilgoe, A. B., Heckenberg, N. R., Nieminen, T. A. & Rubinsztein-Dunlop, H. Phase-transition-like properties of double-beam optical tweezers. *Phys. Rev. Lett.* **107**, 248101 (2011).
13. Juan, M. L., Righini, M. & Quidant, R. Plasmon nano-optical tweezers. *Nature Photon.* **5**, 349–356 (2011).
14. Grigorenko, A. N., Roberts, N. W., Dickinson, M. R. & Zhang, Y. Nanometric optical tweezers based on nanostructured substrates. *Nature Photon.* **2**, 365–370 (2008).
15. Asbury, C. L., Fehr, A. N. & Block, S. M. Kinesin moves by an asymmetric hand-over-hand mechanism. *Science* **302**, 2130–2134 (2003).
16. Bustamante, C., Bryant, Z. & Smith, S. B. Ten years of tension: single-molecule DNA mechanics. *Nature* **421**, 423–427 (2003).
17. Hu, Z., Wang, J. & Liang, J. Manipulation and arrangement of biological and dielectric particles by a lensed fiber probe. *Opt. Express* **12**, 4123–4128 (2004).
18. Liu, Z., Guo, C., Yang, J. & Yuan, L. Tapered fiber optical tweezers for microscopic particle trapping: fabrication and application. *Opt. Express* **14**, 12510–12516 (2006).
19. Yuan, L., Liu, Z. & Yang, J. Measurement approach of Brownian motion force by an abrupt tapered fiber optic tweezers. *Appl. Phys. Lett.* **91**, 054101 (2007).
20. Liberale, C. *et al.* Miniaturized all-fibre probe for three-dimensional optical trapping and manipulation. *Nature Photon.* **1**, 723–727 (2007).
21. Xin, H., Li, X. & Li, B. Massive photothermal trapping and migration of particles by a tapered optical fiber. *Opt. Express* **19**, 17065–17074 (2011).
22. Li, H., Zhang, Y., Li, J. & Qiang, L. Observation of microsphere movement driven by optical pulse. *Opt. Lett.* **36**, 1996–1998 (2011).
23. Hoi, S. K., Hu, Z. B., Yan, Y., Sow, C. H. & Bettiol, A. A. A microfluidic device with integrated optics for microparticle switching. *Appl. Phys. Lett.* **97**, 183501 (2010).
24. Wheeler, D. B., Carpenter, A. E. & Sabatini, D. M. Cell microarrays and RNA interference chip away at gene function. *Nat. Genet.* **37**, S25–S30 (2005).
25. Shi, J. *et al.* Acoustic tweezers: patterning cells and microparticles using standing surface acoustic waves (SSAW). *Lab Chip* **9**, 2890–2895 (2009).
26. Curtis, J. E., Koss, B. A. & Grier, D. G. Dynamic holographic optical tweezers. *Opt. Commun.* **207**, 169–175 (2002).
27. Curtis, J. E. & Grier, D. G. Structure of optical vortices. *Phys. Rev. Lett.* **90**, 133901 (2003).
28. Sun, B., Roichman, Y. & Grier, D. G. Theory of holographic optical trapping. *Opt. Express* **16**, 15765–15776 (2008).
29. Woerdemann, M. *et al.* Dynamic and reversible organization of zeolite L crystals induced by holographic optical tweezers. *Adv. Mater.* **22**, 4176–4179 (2010).
30. Padgett, M. & Di Leonardo, R. Holographic optical tweezers and their relevance to lab on chip devices. *Lab Chip* **11**, 1196–1205 (2011).
31. Righini, M., Zelenina, A. S., Girard, C. & Quidant, R. Parallel and selective trapping in a patterned plasmonic landscape. *Nature Phys.* **3**, 477–480 (2007).
32. Righini, M., Volpe, G., Girard, C., Petrov, D. & Quidant, R. Surface plasmon optical tweezers: tunable optical manipulation in the femtonewton range. *Phys. Rev. Lett.* **100**, 186804 (2008).
33. Gauthier, R. C. Computation of the optical trapping force using an FDTD based technique. *Opt. Express* **13**, 3707–3718 (2005).
34. Xin, H. & Li, B. Targeted delivery and controllable release of nanoparticles using a defect-decorated optical nanofiber. *Opt. Express* **19**, 13285–13290 (2011).
35. Wright, W., Sonek, G. & Berns, M. Radiation trapping forces on microspheres with optical tweezers. *Appl. Phys. Lett.* **63**, 715–717 (1993).
36. Neuman, K. C. & Block, S. M. Optical trapping. *Rev. Sci. Instrum.* **75**, 2787–2809 (2004).

Acknowledgments

The authors thank Dr. Linlin Xu for the fruitful discussion on the FDTD simulation, Prof. Zhigang Cai and Ms. Yayi Li for the experimental assistance. This work was supported by the National Natural Science Foundation of China (Nos. 61205165 and 61007038).

Author contributions

B.L. supervised the project; H.X. performed the simulation and calculation; H.X. and R.X. performed the experiments; H.X. and B.L. discussed the results and wrote the manuscript.

Additional information

Supplementary information accompanies this paper at http://www.nature.com/scientificreports

Competing financial interests: The authors declare no competing financial interests.

How to cite this article: Xin, H., Xu, R. & Li, B. Optical trapping, driving, and arrangement of particles using a tapered fibre probe. *Sci. Rep.* **2**, 818; DOI:10.1038/srep00818 (2012).